Tip-enhanced Raman mapping of local strain in graphene

2015 Nanotechnology 26 175702

(http://iopscience.iop.org/0957-4484/26/17/175702)

IOP Publishing Nanotechnology
Nanotechnology 26 (2015) 175702 (6pp) doi:10.1088/0957-4484/26/17/175702

Tip-enhanced Raman mapping of local strain in graphene

Ryan Beams[1], Luiz Gustavo Cançado[2], Ado Jorio[2], A Nick Vamivakas[1] and Lukas Novotny[3]

[1] Institute of Optics, University of Rochester, Rochester, NY 14627, USA
[2] Departamento de Física, Universidade Federal de Minas Gerais, Belo Horizonte, MG 30123-970, Brazil
[3] ETH Zürich, Photonics Laboratory, 8093 Zürich, Switzerland

E-mail: lnovotny@ethz.ch

Received 15 November 2014, revised 13 February 2015
Accepted for publication 25 February 2015
Published 2 April 2015

Abstract

We demonstrate local strain measurements in graphene by using tip-enhanced Raman spectroscopy (TERS). We find that a single 5 nm particle can induce a radial strain over a lateral distance of ~170 nm. By treating the particle as a point force on a circular membrane, we find that the strain in the radial direction (r) is $\propto r^{-2/3}$, in agreement with force-displacement measurements conducted on suspended graphene flakes. Our results demonstrate that TERS can be used to map out static strain fields at the nanoscale, which are inaccessible using force-displacement techniques.

S Online supplementary data available from stacks.iop.org/nano/26/175702/mmedia

Keywords: Raman scattering, strain, graphene

(Some figures may appear in colour only in the online journal)

1. Introduction

The performance of devices made of two-dimensional (2D) materials such as graphene, boron nitride, and dichalcogenides depends on material strain. Raman spectroscopy has been extensively used to characterize strain in these materials since a mechanical strain causes frequency shifts in several of the Raman bands as well as a widening of the peaks in certain conditions [1–11]. While Raman spectroscopy has played a central role in understanding the mechanical properties of graphene, the studies have been limited to the microscale. The mechanical properties have also been extensively investigated using atomic force microscopy (AFM) based force-displacement techniques on suspended graphene flakes [12]. Since the AFM tip is on the order of 10–20 nm, these studies are able to investigate strains due to local forces, which are inaccessible with conventional, diffraction-limited Raman spectroscopy. As the quality of devices continues to improve, it becomes increasingly important to implement techniques capable of imaging strain distributions at the nanoscale. Recently several works have used tip-enhanced Raman spectroscopy (TERS) on graphene [13–19], illustrating that TERS could be used to create high resolution strain maps.

In this work we demonstrate that TERS can be used to locally measure strain in single layer graphene. We find that a single 5 nm particle leads to a radially strained region on the graphene flake with a radius of ~85 nm and that the strain (ϵ) along the radial direction (r) scales as $\epsilon \propto r^{-2/3}$. This scaling is expected for a circular membrane with a normal force applied at a single point. Our results demonstrate that Raman strain measurements are valid at the nanoscale and are complementary to force-displacement measurements with the benefit of being able to characterize static strain fields intrinsic to a sample. Furthermore nanoscale strains can generate enormous pseudo-magnetic fields in graphene [20] and modify the bandgap in dichalcogenides [21]. Therefore characterizing local strains is crucial for engineering the properties of 2D materials.

2. Results and discussion

The Raman spectrum of graphene consists of three main features: the first-order allowed G band (~1580 cm^{-1}), the G′

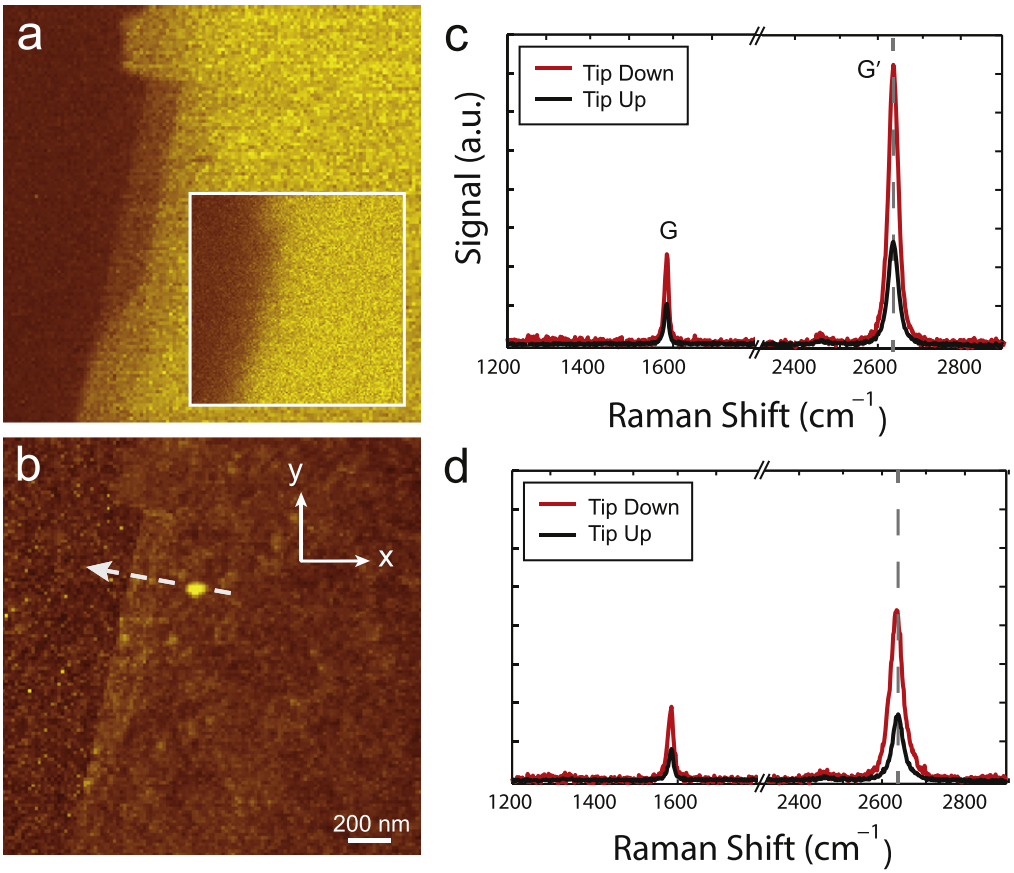

Figure 1. TERS characterization of a graphene sample. (a) TERS image of the G′ band. Inset: confocal image of the same area scaled in intensity by ×2 compared to the TERS image. (b) Simultaneously acquired topography of the flake in (a). The white arrow indicates the location, taken tail to head, of the hyperspectral linescan. (c), (d) Spectra with (red) and without (black) the tip away from and near the particle.

(also called 2D) band (~2700 cm^{-1}), and the defect-induced D band (~1350 cm^{-1}) [22–24]. The G and G′ bands can be used to measure the carrier concentration and strain, with the G band being more sensitive to carrier concentration [25] and the spectral position of the G′ band having a stronger dependence on the strain [1]. The G′ band is also used to determine the number of graphene layers and stacking order [23, 26]. The D band is only present at defect sites in the graphene lattice, which includes edges with armchair chirality [27, 28].

To resolve nanoscale strain fields, we exfoliated a single graphene flake and recorded spatial Raman scattering maps using a near-field microscope as described in [29, 30]. A HeNe laser was used for these measurements and the laser power was kept below 0.5 mW to avoid damaging the tip. The near-field and far-field spectra were acquired with integration times of 30 and 45 s, respectively. Figure 1(a) shows a near-field Raman image of the G′ band. Comparing this TERS image to the confocal scan of the same area (inset), the improvement in resolution and signal is immediately clear. Furthermore, the TERS image reveals that a section of the flake is folded over, as confirmed by the simultaneously acquired topography (figure 1(b)). The spectrum acquired on the folded piece is characteristic of a twisted bilayer graphene flake with a small twist angle [31–33] (see supplementary information). This illustrates that TERS can be used to determine the local stacking order of graphene flakes, which is particularly important due to the growing interest in using 2D heterostructures [34] and twisted multi-layers for engineering opto-electronic properties [31, 32, 35]. In addition to the folded region of the flake, a small particle covered by the graphene sheet is also visible in the topography (figure 1(b)). According to the topographic profile the particle is ~5 nm in height and lifts the graphene lattice over an area of ~170 nm.

To investigate local strain we acquired a hyperspectral Raman linescan along the white line (tail to head) in figure 1(b). The flake was scanned underneath the stationary, laser-irradiated gold tip, and a spectrum was acquired at each location. Figures 1(c) and (d) show example spectra acquired away from and near the particle, respectively, with the tip down (red) and retracted (black). Figures 2(a)–(e) show plots of the hyperspectral linescan for the center frequency and the width of the G and G′ bands as well as the D band amplitude after fitting each peak with a single Lorentzian. The vertical dashed lines indicate the edges of the folded region and the vertical solid line is the location of the particle. Three important features are visible in the linescans. First, two D band peaks are observed, which are localized at the two edges of the bilayer region as expected [17, 28, 36, 37]. The D band linescan was normalized by the maximum far-field value to

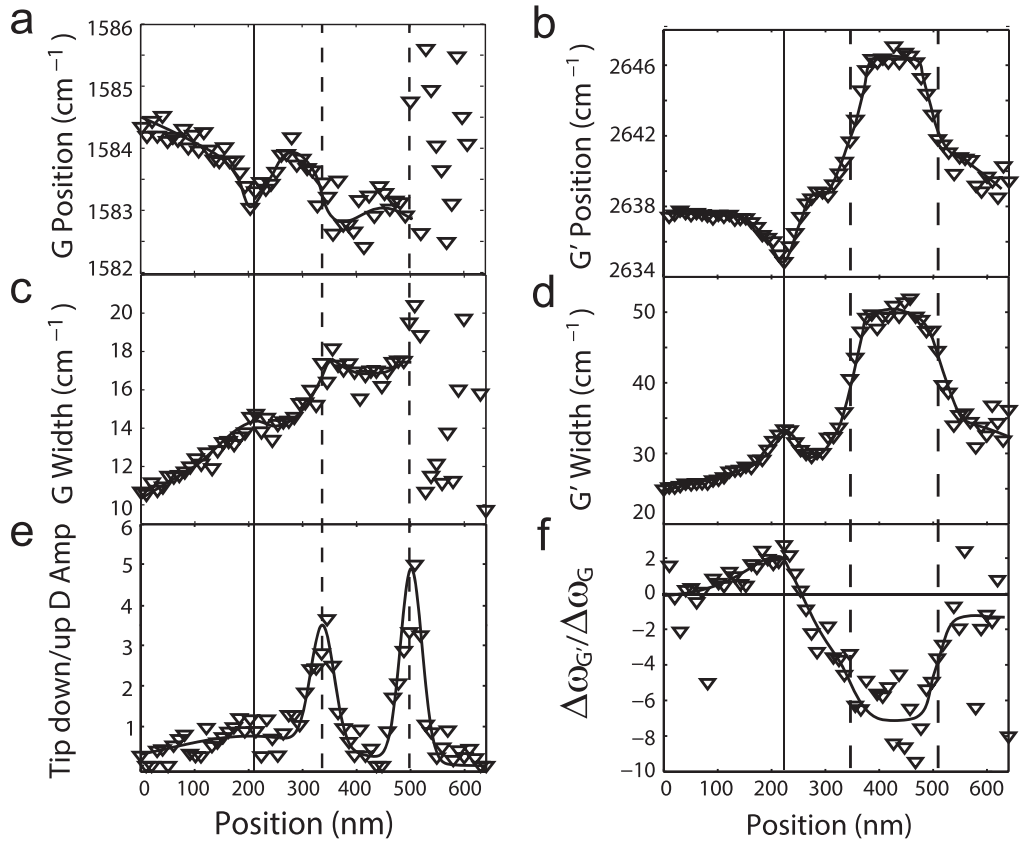

Figure 2. (a), (b) Center frequency of the G and G′ bands, respectively. (c), (d) Width of the G and G′ bands, respectively. (e) D band amplitude. (f) Ratio of the Raman shifts for the G′ and G band, $\Delta\omega_{G'}/\Delta\omega_G$. The black lines are guides for the eye.

accentuate the enhancement. The measured width of the D band intensity profile is a convolution of the tip with the spatial extent of the D band (∼4 nm) [17, 28, 37]. Second, in the bilayer region (after ∼350 nm) the G′ band blueshifts (figure 2(b)) and the width drastically increases (figure 2(d)), as expected [22, 23, 32, 38, 39]. Finally, there is a kink in the G and G′ band position and width around 200 nm, which corresponds to the location of the particle in figures 2(a)–(d). The redshift of the G and G′ bands as well as the G′ band broadening of ≈4 cm^{-1} indicate that the particle locally strains the graphene flake as one would intuitively expect. While variations in carrier concentrations can also shift the Raman bands, this shift cannot be due to doping since the observed shift is larger for the G′ band than for the G band [25]. Furthermore, for both peaks to redshift the flake must be more strongly p-doped away from the particle than on the particle. In this case the ratio of the amplitudes, $I(G')/I(G)$, would increase [25], which is not observed. Therefore we conclude that strain, not doping, is responsible for the observed shift. This is further corroborated by the ratio of the Raman shifts, $\Delta\omega_{G'}/\Delta\omega_G$, shown in figure 2(f), which was previously shown to be ≈2.2 for strained single layer graphene in good agreement with our measurements near the particle [7, 9, 11].

The two types of strain that are most commonly studied using Raman spectroscopy are uniaxial and biaxial strain. As mentioned earlier, under tensile strain the G and G′ bands redshift. For uniaxial strain the G band splits into two peaks and the G′ band can broaden or split [1, 4, 40, 41]. The amount that the G′ band broadens or splits depends on the magnitude of strain and the direction of the incident polarization relative to the strain axis [4, 40]. In contrast, the widths of the G and G′ bands are unaffected by biaxial strain [3, 9]. In our case the particle applies a localized force on the graphene flake, which leads to a radial strain. In other words the strain is maximum at the location of the particle and decreases radially outward. This type of strain has been investigated using force-displacement measurements on graphene suspended over holes [12, 42, 43].

At first glance radial strain may seem similar to biaxial strain, in which case the observed broadening of the G′ band is surprising. However, radial strain should split the G′ band as well since at any position, r, the graphene lattice experiences strain along a single direction that modifies the band structure, similar to uniaxial strain. Unlike uniaxial strain, for radial strain the strain axis relative to the crystal axes changes with the polar angle (θ) and leads to a θ-dependent broadening or splitting. In our case we observe broadening, not splitting, which can be attributed to several factors. First, based on the Raman shift, the strain is not significant enough to split the G′ band. Second, in our measurements the near-field probe behaves as a vertical dipole perpendicular to the graphene surface [18, 44]. Therefore the measured spectra are an average of all excitation polarizations within near-field

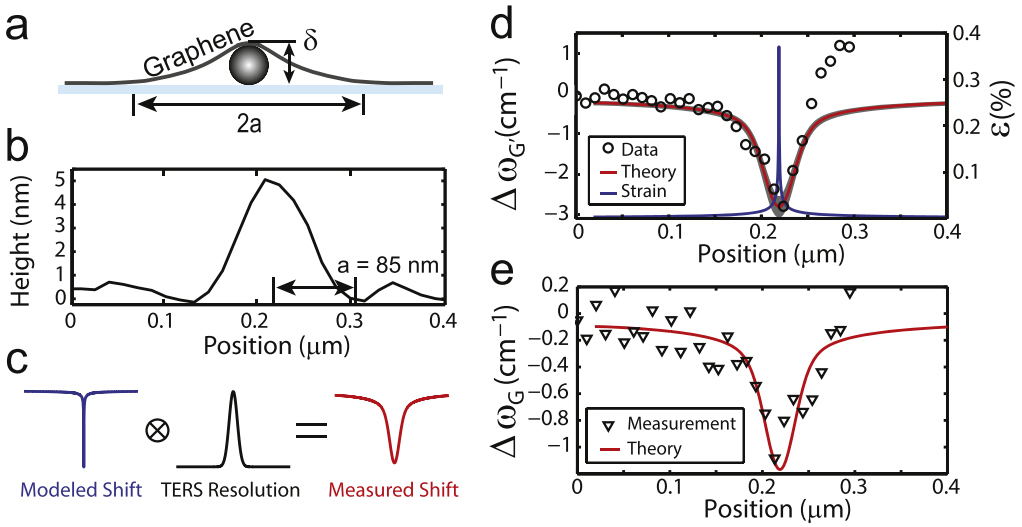

Figure 3. Illustration and measurements of a radially strained graphene flake. (a) Sketch of a particle straining the graphene. (b) Topographic profile of the strained region. (c) Schematic of the convolution of the TERS resolution (black) with the modeled Raman shift (blue) to give the measured Raman shift (red). (d) Plot of the Raman shift of the G′ band, $\Delta\,\omega_{G'}$ (circles) from figure 2(b). The fit is shown in red and the total strain profile, ϵ, is shown in blue. (e) Plot of the Raman shift of the G band, $\Delta\,\omega_{G'}$ (triangles) from figure 2(a). A strain of $\epsilon = 0.37\%$ was used for fitting of the Raman data in both (d) and (e).

interaction areas, which adds additional broadening to the G′ band.

In order to gain a more quantitative understanding, the strain can be related to the Raman shift ($\Delta\omega$) for each band through the Grüneisen parameter (γ) for that band using the equation

$$\Delta\omega = -\omega_0\,\gamma\,\epsilon = -\omega_0\,\gamma\,(\epsilon_r + \epsilon_\theta), \tag{1}$$

where ω_0 is the unshifted frequency. In this case ϵ has been written in polar coordinates so that the principal components are ϵ_r and ϵ_θ along the radial and circumferential directions, respectively. In the absence of shearing strains, the total strain is $\epsilon = \epsilon_r + \epsilon_\theta$, known as the hydrostatic strain [1, 45]. We used $\gamma_{G'} = 2.6$ and $\gamma_G = 1.8$ for the Grüneisen parameters [9].

In order to characterize the radial and circumferential strains due to the particle, the graphene flake can be treated as a clamped circular membrane with a point load force applied in the center. A sketch of the strained graphene is shown in figure 3(a). As long as the displacement force is sufficiently localized, it can be treated as a point load. Mathematically, the point load model is valid if $\delta \ll 2a$, where δ is the diameter of the object applying the force and a is the radial extent of the strain [42]. In our case $\delta = 5$ and $a = 85$ nm, δ being defined by the diameter of the particle. Figure 3(b) shows the topographic profile of the graphene over the particle. Assuming a point load model, the applied force, F, has a linear deflection term proportional to the pre-stress of the flake and a non-linear deflection term [12]. The pre-stress varies depending on the processing of the sample and the substrate, but it is typically less than a few GPa [12]. For simplicity, we assume zero pre-stress in which case F can be approximated as

$$F = E\,(q^3 a h)\left(\frac{\delta}{a}\right)^3, \tag{2}$$

where h is the membrane thickness, and E is the Young's modulus. The parameter q is defined as $q = 1/(1.05 - 0.15\nu - 0.16\nu^2)$, where ν is the Poisson ratio [12, 43]. In the case of graphene $h = 0.335$ nm, $E = 1$ TPa, and $\nu = 0.165$ [12, 42, 43]. Often E is redefined for 2D materials by grouping them with h to have units of Nm^{-1} [12]. In the case of zero pre-strain, also known as Schwerin's solution [43], the applied force leads to radial and circumferential strains described by [43, 46]

$$\epsilon_r = \frac{3-\nu}{4}\left(\frac{F^2}{3\pi^2 E^2\,h^2}\right)^{1/3}\left(\frac{1}{r}\right)^{2/3}$$
$$\epsilon_\theta = \frac{1-3\nu}{4}\left(\frac{F^2}{3\pi^2 E^2\,h^2}\right)^{1/3}\left(\frac{1}{r}\right)^{2/3}. \tag{3}$$

These equations illustrate that radial and circumferential strains are significantly different than uniaxial or biaxial strains that are typically studied using Raman spectroscopy. Uniaxial strain is uniform along the strain direction and biaxial strain is isotropic. However, radial and circumferential strains reach a maximum in the center and decrease away from the applied point force. Note that according to equation (3), ϵ_r is more than a factor five larger than ϵ_θ for graphene.

The Raman measurements in figure 2 show that the strain has a gradient over the particle, as expected according to equation (3). Figures 3(d), (e) show a zoomed-in plot of the G and G′ shift from figures 2(a) and (b). The strain profile can be calculated by substituting equation (2) into equation (3). The Raman shift can then be calculated by substituting the strain profile from equation (3) into equation (1). This result will be referred to as the modeled Raman shift profile. The measured Raman shift profile is a convolution of the actual Raman shift profile with the TERS resolution profile.

Therefore to test the validity of strain model presented above, the resolution of the tip must be known in order to convolve it with the modeled Raman shift profile. The resolution of the tip was estimated from the D band spatial profile. In this case the D band profile from the single layer region of the flake in figure 1(a) was used because the Raman behavior at the edge of a single layer flake has been extensively studied [17, 28, 37]. The tip profile was treated as a Gaussian with a FWHM of 34 nm. This resolution is sufficient to resolve the strain due to the particle (see supplementary information). Convolving this Gaussian with the modeled Raman shift profile gives the expected theoretical Raman shift profile, which can be compared with the measurements. This process is depicted in figure 3(c). One important note is that equation (3) is singular at the location of the particle ($r = 0$). To avoid this issue we used the maximum shift from Raman measurements to scale the amplitude of the modeled Raman shift profile, which resulted in a maximum strain of $\epsilon = 0.37\%$ on the particle. It is important to note that the pre-strain of the flake could change the magnitude of the calculated strain, which is not included in the model presented in equation (3). The resulting theoretical Raman shift and strain profiles are shown in figure 3(d) in red and blue, respectively. The theoretical Raman shift profile is in good agreement with the measurements and illustrates that $\epsilon \propto r^{-2/3}$. The asymmetry on the right side of the plotted data is due to the presence of the bilayer region shifting the G′ frequency near the fold. The shaded gray area is the resulting shift due a strain between $\epsilon = 0.34$ and 0.40% and illustrates the sensitivity of Raman spectroscopy to strain. The fitting for the G band data using a maximum strain of $\epsilon = 0.37\%$ is shown in figure 3(e). A comparison with other fitting functions is shown in the supplementary information.

3. Summary

We have shown that TERS can measure the local strain in a graphene flake. We observed a strain of ∼0.37% due to a 5 nm particle under the flake. These results demonstrate that Raman spectroscopy is a valid strain characterization tool at the nanoscale and that the strain due to an isolated particle is $\propto r^{-2/3}$. TERS can provide significant insights into the nanoscale properties of a graphene flake, which will become increasingly important as the dimensions of graphene devices continue to decrease. While this was demonstrated on graphene, this type of characterization is applicable to a wide variety of devices in the newly emerging field of 2D heterostructures.

Acknowledgments

We thank TW Johnson and S-H Oh for fabricating the near-field probes and A Kitt for his valuable insights. AJ acknowledges CAPES for financing his stay at ETH. AJ and LGC acknowledge financial support from CNPq and FAPEMIG. LN acknowledges the financial support by the US Department of Energy (grant DE-FG02-05ER46207) and the Swiss National Science Foundation (grant 200021_149433).

References

[1] Mohiuddin T M G *et al* 2009 Uniaxial strain in graphene by Raman spectroscopy: G peak splitting, Grüneisen parameters, and sample orientation *Phys. Rev.* B **79** 205433
[2] Metzger C, Rémi S, Liu M, Kusminskiy S V, Neto A H C, Swan A K and Goldberg B B 2009 Biaxial strain in graphene adhered to shallow depressions *Nano Lett.* **10** 6–10
[3] Ding F, Ji H, Chen Y, Herklotz A, Dörr K, Mei Y, Rastelli A and Schmidt O G 2010 Stretchable graphene: a close look at fundamental parameters through biaxial straining *Nano Lett.* **10** 3453–8
[4] Huang M, Yan H, Heinz T F and Hone J 2010 Probing strain-induced electronic structure change in graphene by Raman spectroscopy *Nano Lett.* **10** 4074–9
[5] Frank O, Tsoukleri G, Riaz I, Papagelis K, Parthenios J, Ferrari A C, Geim A K, Novoselov K S and Galiotis C 2011 Development of a universal stress sensor for graphene and carbon fibres *Nat. Commun.* **2** 255
[6] Cheng Y C, Zhu Z Y, Huang G S and Schwingenschlögl U 2011 Grüneisen parameter of the G mode of strained monolayer graphene *Phys. Rev.* B **83** 115449
[7] Lee J E, Ahn G, Shim J, Lee Y S and Ryu S 2012 Optical separation of mechanical strain from charge doping in graphene *Nat. Commun.* **3** 1024
[8] Lee J-U, Yoon D and Cheong H 2012 Estimation Young's of modulus of graphene by Raman spectroscopy *Nano Lett.* **12** 4444–8
[9] Zabel J, Nair R R, Ott A, Georgiou T, Geim A K, Novoselov K S and Casiraghi C 2012 Raman spectroscopy of graphene and bilayer under biaxial strain: bubbles and balloons *Nano Lett.* **12** 617–21
[10] Kitt A L, Qi Z, Rémi S, Park H S, Swan A K and Goldberg B B 2013 How graphene slides: measurement and theory of strain-dependent frictional forces between graphene and SiO_2 *Nano Lett.* **13** 2605–10
[11] Metten D, Federspiel F, Romeo M and Berciaud S 2014 All-optical blister test of suspended graphene using micro-Raman spectroscopy *Phys. Rev. Appl.* **2** 054008
[12] Lee C, Wei X, Kysar J W and Hone J 2008 Measurement of the elastic properties and intrinsic strength of monolayer graphene *Science* **321** 385–8
[13] Saito Y, Verma P, Masui K, Inouye Y and Kawata S 2009 Nano-scale analysis of graphene layers by tip-enhanced near-field raman spectroscopy *J. Raman Spectrosc.* **40** 1434–40
[14] Stadler J, Schmid T and Zenobi R 2011 Nanoscale chemical imaging of single-layer graphene *ACS Nano* **5** 8442–8
[15] Ghislandi M, Hoffmann G G, Tkalya E, Xue L and de With G 2012 Tip-enhanced Raman spectroscopy and mapping of graphene sheets *Appl. Spectrosc. Rev.* **47** 371–81
[16] Ikeda K, Takase M, Hayazawa N, Kawata S, Murakoshi K and Uosaki K 2013 Plasmonically nanoconfined light probing invisible phonon modes in defect-free graphene *J. Am. Chem. Soc.* **135** 11489–92
[17] Su W and Roy D 2013 Visualizing graphene edges using tip-enhanced Raman spectroscopy *J. Vac. Sci. Technol.* B **31** 041808
[18] Cançado L G, Beams R, Jorio A and Novotny L 2014 Theory of spatial coherence in near-field Raman scattering *Phys. Rev.* X **4** 031054

[19] Beams R, Cançado L G, Oh S-H, Jorio A and Novotny L 2014 Spatial coherence in near-field Raman scattering *Phys. Rev. Lett.* **113** 186101
[20] Levy N, Burke S A, Meaker K L, Panlasigui M, Zettl A, Guinea F, Neto A H C and Crommie M F 2010 Strain-induced pseudo-magnetic fields greater than 300 tesla in graphene nanobubbles *Science* **329** 544–7
[21] Castellanos-Gomez A, Roldán R, Cappelluti E, Buscema M, Guinea F, van der Zant H S J and Steele G A 2013 Local strain engineering in atomically thin MoS_2 *Nano Lett.* **13** 5361–6
[22] Ferrari A C *et al* 2006 Raman spectrum of graphene and graphene layers *Phys. Rev. Lett.* **97** 187401
[23] Malard L M, Pimenta M A, Dresselhaus G and Dresselhaus M S 2009 Raman spectroscopy in graphene *Phys. Rep.* **473** 51–87
[24] Jorio A, Dresselhaus M S, Saito R and Dresselhaus G 2011 *Raman Spectroscopy in Graphene Related System* 1st edn (Weinheim: Wiley)
[25] Das A *et al* 2008 Monitoring dopants by Raman scattering in an electrochemically top-gated graphene transistor *Nat. Nanotechnology* **3** 210
[26] Poncharal P, Ayari A, Michel T and Sauvajol J-L 2008 Raman spectra of misoriented bilayer graphene *Phys. Rev.* B **78** 113407
[27] Cançado L G, Pimenta M A, Neves B R A, Dantas M S S and Jorio A 2004 Influence of the atomic structure on the Raman spectra of graphite edges *Phys. Rev. Lett.* **93** 247401
[28] Casiraghi C, Hartschuh A, Qian H, Piscanec S, Georgi C, Fasoli A, Novoselov K S, Basko D M and Ferrari A C 2009 Raman spectroscopy of graphene edges *Nano Lett.* **9** 1433–41
[29] Hartschuh A 2008 Tip-enhanced near-field optical microscopy *Angew. Chem., Int. Ed.* **47** 8178–91
[30] Johnson T W, Lapin Z J, Beams R, Lindquist N C, Rodrigo S G, Novotny L and Oh S-H 2012 Highly reproducible near-field optical imaging with sub-20 nm resolution based on template-stripped gold pyramids *ACS Nano* **6** 9168–74
[31] Carozo V, Almeida C M, Ferreira E H M, Cançado L G, Achete C A and Jorio A 2011 Raman signature of graphene superlattices *Nano Lett.* **11** 4527–34
[32] Kim K, Coh S, Tan L Z, Regan W, Yuk J M, Chatterjee E, Crommie M F, Cohen M L, Louie S G and Zettl A 2012 Raman spectroscopy study of rotated double-layer graphene: Misorientation-angle dependence of electronic structure *Phys. Rev. Lett.* **108** 246103
[33] Carozo V *et al* 2013 Resonance effects on the Raman spectra of graphene superlattices *Phys. Rev.* B **88** 085401
[34] Geim A and Grigorieva I 2013 Van der Waals heterostructures *Nature* **499** 419–25
[35] Wang Y *et al* 2013 Resonance Raman spectroscopy of G-line and folded phonons in twisted bilayer graphene with large rotation angles *Appl. Phys. Lett.* **103** 123101
[36] Lucchese M M, Stavale F, Ferreira E H M, Vilani C, Moutinho M V O, Capaz R B, Achete C A and Jorio A 2010 Quantifying ion-induced defects and Raman relaxation length in graphene *Carbon* **48** 1592–7
[37] Beams R, Cançado L G and Novotny L 2011 Low temperature Raman study of the electron coherence length near graphene edges *Nano Lett.* **11** 1177–81
[38] Malard L M, Nilsson J, Elias D C, Brant J C, Plentz F, Alves E S, Neto A H C and Pimenta M A 2007 Probing the electronic structure of bilayer graphene by Raman scattering *Phys. Rev.* B **76** 201401
[39] Hao Y, Wang Y, Wang L, Ni Z, Wang Z, Wang R, Koo C K, Shen Z and Thong J T L 2010 Probing layer number and stacking order of few-layer graphene by Raman spectroscopy *Small* **6** 195–200
[40] Frank O *et al* 2011 Raman 2D-band splitting in graphene: theory and experiment *ACS Nano* **5** 2231–9
[41] Shioya H, Craciun M F, Russo S, Yamamoto M and Tarucha S 2014 Straining graphene using thin film shrinkage methods *Nano Lett.* **14** 1158–63
[42] Tan X, Wu J, Zhang K, Peng X, Sun L and Zhong J 2013 Nanoindentation models and Young's modulus of monolayer graphene: a molecular dynamics study *Appl. Phys. Lett.* **102** 071908
[43] Komaragiri U, Begley M R and Simmonds J G 2005 The mechanical response of freestanding circular elastic films under point and pressure loads *J. Appl. Mech.* **72** 203–12
[44] Maximiano R V, Beams R, Novotny L, Jorio A and Caçado L G 2012 Mechanism of near-field Raman enhancement in two-dimensional systems *Phys. Rev.* B **85** 235434
[45] Grimvall G 1999 *Thermophysical Properties of Materials* (Amsterdam: Elsevier)
[46] Yamamoto M, Pierre-Louis O, Huang J, Fuhrer M S, Einstein T L and Cullen W G 2012 'The princess and the pea' at the nanoscale: wrinkling and delamination of graphene on nanoparticles *Phys. Rev.* X **2** 041018